


# Fully automated MR liver volumetry using watershed segmentation coupled with active contouring

Hieu Trung Huynh<sup>1</sup>  · Ngoc Le-Trong<sup>1,2</sup> · Pham The Bao<sup>2,3</sup> · AYTEK Oto<sup>4</sup> · Kenji Suzuki<sup>5</sup>

Received: 14 June 2016 / Accepted: 28 October 2016 / Published online: 21 November 2016  
© CARS 2016

## Abstract

**Purpose** Our purpose is to develop a *fully* automated scheme for liver volume measurement in abdominal MR images, without requiring any user input or interaction.

**Methods** The proposed scheme is fully automatic for liver volumetry from 3D abdominal MR images, and it consists of three main stages: preprocessing, rough liver shape generation, and liver extraction. The preprocessing stage reduced noise and enhanced the liver boundaries in 3D abdominal MR images. The rough liver shape was revealed fully automatically by using the watershed segmentation, thresholding transform, morphological operations, and statistical properties of the liver. An active contour model was applied to refine the rough liver shape to precisely obtain the liver boundaries. The liver volumes calculated by the proposed scheme were compared to the “gold standard” references which were estimated by an expert abdominal radiologist.

**Results** The liver volumes computed by using our developed scheme excellently agreed (Intra-class correlation coefficient was 0.94) with the “gold standard” manual volumes by the radiologist in the evaluation with 27 cases from multiple

medical centers. The running time was 8.4 min per case on average.

**Conclusions** We developed a *fully* automated liver volumetry scheme in MR, which does not require any interaction by users. It was evaluated with cases from multiple medical centers. The liver volumetry performance of our developed system was comparable to that of the gold standard manual volumetry, and it saved radiologists’ time for manual liver volumetry of 24.7 min per case.

**Keywords** Fully automated segmentation scheme · Liver volumetry · Quantitative radiology · MR liver volumetry · Transplantation

## Introduction

The transplantation of the liver improves significantly the survival rate of patients with liver diseases. One of the crucial factors contributed to the success of a transplantation procedure is the liver volume, because both a donor and a recipient must keep a certain amount of the liver for living [1]. Hence, the liver volumetry plays an important role for planning the treatment of various liver diseases. Liver volume estimation is performed by a manual volumetry method. This method can offer accurate results, but it is tedious and time-consuming. It is also subjective: there are inter-observer variations among different radiologists and intra-observer variations within the same radiologist. To address those problems, investigators developed computerized methods for liver volumetry by using image analysis and machine-learning techniques.

Several computerized schemes have been developed for liver segmentation on CT images [2–4]. In comparison with CT images, only a few schemes were proposed for computer-

---

✉ Hieu Trung Huynh  
hthieu@ieee.org

<sup>1</sup> Faculty of Information Technology, Industrial University of Ho Chi Minh City, Ho Chi Minh City, Vietnam

<sup>2</sup> Faculty of Information Technology, University of Science, Ho Chi Minh City, Vietnam

<sup>3</sup> Faculty of Mathematics and Computer Science, University of Science, Ho Chi Minh City, Vietnam

<sup>4</sup> Department of Radiology, The University of Chicago, Chicago, IL 60637, USA

<sup>5</sup> Medical Imaging Research Center, Illinois Institute of Technology, Chicago, IL 60616, USA

ized liver volumetry on MR images [5]. A recently published paper [6] proposed a variational level set-based method for liver segmentation using Sobolev gradient. This method was evaluated with different MR images, which are spectral pre-saturation inversion recovery (SPIR) images. Gloger et al. [7] developed a scheme combining available information from different MR weightings. Their scheme consisted of a probability map, multiclass linear discriminant analysis (LDA), a region-growing technique, and a thresholding technique. Their scheme was evaluated on 20 normal and ten fatty liver cases. Rusko et al. [8] proposed a segmentation scheme based on the intensity; this scheme uses different probabilistic models to represent the different parts of liver, which can catch the local intensity differences better. This scheme was tested on eight cases. Masoumi et al. [9] proposed an approach using an iterative watershed algorithm and neural networks. In this method, six neural networks which were trained by a backpropagation algorithm were used to extract the features of the liver region. These features were employed to monitor the quality of segmentation using a watershed transform. The parameters were adjusted in several iterations. In our previous studies, the approaches for liver segmentation based on a fast marching algorithm and a geodesic active contour were presented [10]. The performance of these approaches was tested on 23 cases from a single hospital. This is a semi-automated scheme that requires 5–8 initial seed points. Choosing the seed points in MR images may affect the final results. We presented a preliminary fully automatic scheme using the histogram and a level set algorithm at a meeting [11]. The performance of the preliminary scheme was tested on only 10 cases in a single hospital. In this method, the rough shape of liver was determined based on the second-to-last peak of the histogram. However, since the peak corresponding to the intensity distribution of the liver may vary by different cases due to variations of MR images, the robustness against case variations was limited.

Although the above studies showed promising results, the computerized liver volumetry on MR images is still a challenging task in medical image analysis. The liver tissue intensities are similar to the intensities of other organs, which are not easy to distinguish the liver from adjacent organs and tissues. The 3D MR images typically have the variations of contrast and edge magnitudes, which is complicate to apply the edge-based segmentation and limited to apply the histogram based method. Some level set-based techniques require the initial seed points chosen manually, which may be time-consuming. The *fully* automated liver volumetry is a technical challenge that has not been resolved adequately. In this study, we rose to the challenge and developed a *fully* automated scheme for liver volumetry in MR images, based on the combination of the watershed transform and the active contour model, without requiring any user input or interaction. We evaluated our developed scheme with cases from

multiple medical centers, which offered more critical evaluation, compared to evaluation with single center cases.

## Materials and methods

### Liver MRI cases

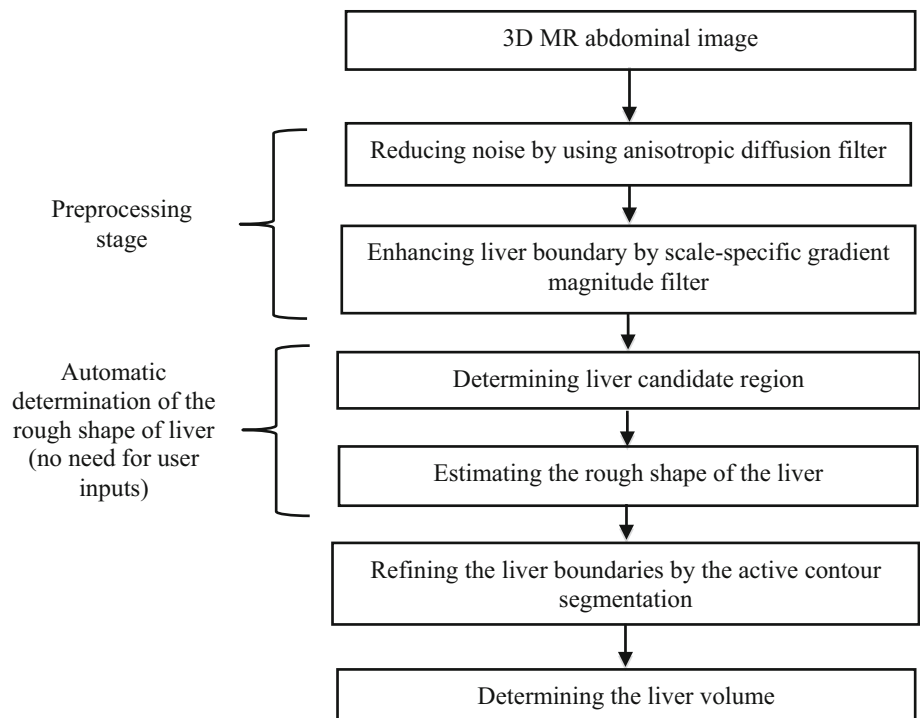
The dataset consisted of 27 cases of 3D MRI scans obtained from multiple medical centers. Sixteen cases were obtained from 16 patients by using the 1.5T MRI scanners (Sigma HDxt/HDx; Achieva, Philips medical systems, Cleveland, OH; and GE medical systems, Milwaukee, WI) at the University of Chicago Medical center. The intravenous gadolinium-based contrast agents (8–20 mL; mean  $15.3 \pm 4.2$  mL) were administrated to patients. Eleven other cases were obtained from 11 patients with MRI scanners (Avanto, Siemens) at the Medic Medical center. With the Siemens system, the post-contrast MR images were generated by using the T1-weighted VIBE sequence (volumetrically-interpolated breath-hold examination). With the GE and Philips systems, they were generated by the T1-weighted LAVA (liver acquisition with volume acceleration) or THRIVE (high-resolution isotropic volume examination) sequence. The repetition time (TR) was from 3.48 to 4.74, the echo time (TE) was from 1.64 to 2.38, and the flip angle was  $10^\circ$ . The slice thickness or collimation was 5 and 4 mm for the GE and the Philips system, respectively, and it was from 3.5 to 4 mm for the Siemens one. The reconstruction interval was 2.5 and 2 mm for the GE and the Philips system, respectively, and it was 1 mm for the Siemens one. The MR slice number was 100 in average (min 88, max 120) for the GE and Philips system, and it was 55 in average (min 44, max 56) for the Siemens system. The matrix size for each MR slice was  $256 \times 256$ ,  $320 \times 230$ ,  $384 \times 384$ , or  $512 \times 512$  pixels, and the voxel size was ranging from 1.17 to 1.72 mm on the  $x$  and  $y$  axes. Our dataset consists of cases with the liver diseases.

In order to compute the “gold standard” liver volumes, a board-certified abdominal radiologist traced carefully contours on each slice which contains the liver tissues. The volume of the liver corresponding to each slice was determined by multiplying the liver region areas to the reconstruction interval. Note that the successive slices were overlapped and the slice thickness was different from the reconstruction interval. The liver volumes in all slices were summed to obtain the total volume of the liver. The tracing time for each case was recorded. The performance evaluation of the proposed scheme was performed by comparison with the “gold standard” liver volumes.

### Computerized scheme for MR liver volumetry

The studies for the computerized liver volumetry on MR image were investigated by our group. In those studies, the

**Fig. 1** Overview of the fully automated scheme for computerized liver volumetry in MR images



proposed scheme employed the fast marching algorithm to determine the initial surface of the liver, and then this surface was refined by employing the geodesic active contour. The fast marching algorithm requires the initial seed points chosen manually, which may affect the final results and be time-consuming. Another automatic scheme also was developed in our previous study [11]. This scheme determined the rough shape of the liver based on the second-to-last peak of the histogram. However, the peak corresponding to the intensity distribution of the liver may vary by different cases due to variations of MR images, which leads to the limitation in the robustness against case variations.

In this study, we developed a *fully* automated segmentation scheme for measuring the liver volume in 3D abdominal MR image. The proposed scheme includes three main stages: preprocessing, automatic estimation of the rough liver shape, and liver extraction as depicted in Fig. 1. First, noise in 3D MR image  $I$  is reduced by using an anisotropic diffusion filter. This filter is controlled by a modified curvature diffusion equation (MCDE) given by

$$I_t = |\nabla I| \nabla \cdot c(|\nabla I|) \frac{\nabla I}{|\nabla I|}, \tag{1}$$

where  $c(\cdot)$  is the diffusion parameter determined by  $c(|\nabla I|) = e^{-\left(\frac{|\nabla I|}{K}\right)^2}$ , and  $K$  is a conductance parameter. This filter smooths the image while preserving major structures including liver boundaries. A recursive filtering method with the Gaussian kernel was applied to the smoothed image to generate the image  $I_G$  which enhances edges. The gradient

magnitude image is generated, in which each voxel is determined by

$$I_M = \sqrt{\left(\frac{\partial I_G}{\partial x}\right)^2 + \left(\frac{\partial I_G}{\partial y}\right)^2 + \left(\frac{\partial I_G}{\partial z}\right)^2}. \tag{2}$$

In this study, the intensity range of the liver is estimated based on the watershed transform and the statistical characteristics of the liver. The height function obtained from the gradient magnitude image is used as the input to the watershed transform. The main goal of this transform is to find the catchment basins which are associated with the local extremes of the height function. The local extremes are formed based on geometric structures where the boundaries are indicated by the higher values of the height function. The watershed segmentation divides the image into separated regions. These regions are labeled, which indicates the membership of a voxel in a particular region.

Let  $G = \{G_1, G_2, \dots, G_M\}$  be a list of labeled regions with the decreasing order of volumes, i.e.,  $\text{vol}(G_i) \geq \text{vol}(G_{i+1}), i = 1, \dots, M - 1$ . The  $x$  coordinate of the centroid corresponding to region  $G_i$  is calculated by

$$C_i^x = \frac{\sum_{\mathbf{p} \in G_i} x I(\mathbf{p})}{\sum_{\mathbf{p} \in G_i} I(\mathbf{p})}. \tag{3}$$

Because the liver region candidate usually locates on the left part of the image, its centroid satisfies  $C_i^x \leq X_I/2$ , where  $X_I$  is the size of the image on the  $x$ -axis. The length of the

axes of the hyper-ellipsoid which fits to a region  $G_i$  can be determined as  $4\sqrt{\lambda_j^i}$ , where  $\lambda_j^i$ ,  $j = 1, 2, 3$  are eigenvalues corresponding to  $G_i$  in the descending order. Note that as the eigenvalues are in the descending order, the axis lengths will correspond to the decreasing lengths of the hyper-ellipsoid axes. The volume ratio between region  $G_i$  and its oriented bounding box is calculated by

$$r_i = \frac{\text{vol}(G_i)}{64 \prod_{j=1}^3 \lambda_j^i}. \quad (4)$$

From the statistical characteristics of the liver, region  $G_1$  evolving the liver candidate is one of the first five regions of  $G$  (except the background regions) and satisfies

$$l = \underset{i}{\text{argmax}} r_i \quad \text{and} \quad C_i^x \leq X_I/2. \quad (5)$$

The steps in the fully automatic determination of liver candidate regions can be summarized as follows:

*Input* Given  $G = \{G_1, G_2, \dots, G_M\}$  be a list of labeled regions with the decreasing order of volumes.

*Output* The index of a region ( $l$ ) which is a liver candidate.

*Step 1* Initialize the maximum volume ratio ( $\text{max\_ratio}=0$ ) and its corresponding index ( $l = 0$ )

*Step 2* Let  $i$  loop over values [1,5], for each  $G_i$ :

    Compute the  $x$ -coordinate of the weighted centroid ( $C_i^x$ ) by using (3).

    Compute the volume ratio ( $r_i$ ) by using (4).

    If  $r_i > \text{max\_ratio}$  and  $C_i^x \leq X_I/2$

        Update the maximum volume ratio ( $\text{max\_ratio}=r_i$ ) and its corresponding index ( $l = i$ )

*Step 3* Return the output value  $l$ .

Due to variations of the intensities in an MR image,  $G_1$  may not approximate the liver well, but it can infer the intensity range of the liver in the image. Let  $lpk$  and  $\sigma$  be mean and variation of the intensities in  $G_1$ . Two thresholds are computed by

$$\text{Lower threshold} = lpk - m\sigma$$

$$\text{Upper threshold} = lpk + m\sigma, \quad (6)$$

where  $m$  is a user-defined parameter. The thresholding method is applied to the image  $I$  with above two thresholds to generate the thresholding image  $I_{th}$ . The image  $I_{th}$  then is updated by

$$I_u(\mathbf{p}) = u(I_{th}(\mathbf{p})) + g(\mathbf{p}), \quad (7)$$

where  $g$  and  $u$  are the member and unit step function defined by

$$g(\mathbf{p}) = \begin{cases} 1 & \text{if } \mathbf{p} \in G_1 \\ 0 & \text{otherwise} \end{cases} \quad \text{and} \quad u(x) = \begin{cases} 1 & \text{if } x > 0 \\ 0 & \text{otherwise} \end{cases} \quad (8)$$

The image  $I_u$  may include the liver and other organs because their intensities are similar to those of the liver. The boundaries between these organs and the liver are enhanced by

$$I_e(\mathbf{p}) = I_u(\mathbf{p})u(I_M(\mathbf{p}) - \theta), \quad (9)$$

where  $\theta$  is a user-defined parameter. Morphological opening and connected-component operations [12, 13] are applied to separate the organs. The region with the largest volume is filtered out. Then the morphological operation is applied to this region to generate the initial shape of the liver.

The initial shape is refined by employing a geodesic active contour model [14]. This model refines the boundaries by combining the classical snake approach which is based on the energy minimization and the geometric active contours which is based on the curve evolution theory. The curve evolution is represented by using the level set approach, and its evolution is governed by a partial differential equation:

$$\frac{d\varphi}{dt} = \alpha F(\mathbf{p})\kappa |\nabla\varphi| - \beta S(\mathbf{p}) |\nabla\varphi| - \gamma A(\mathbf{p}) \cdot \nabla\varphi, \quad (10)$$

where  $\varphi(\mathbf{p}, t)$  is a level set function, the first term is the mean curvature which is based on a spatial modifier  $F(\cdot)$  and the mean curvature  $\kappa$ ,  $S(\cdot)$  is an expansion or propagation function, and  $A(\cdot)$  is an advection vector function. The mean curvature term governs the smoothness of the surface (front). The front moves in the direction which decreases the total curvature; therefore, the regions with the high curvature areas are smoothed out. The expansion function controls the propagation speed of a front. The coefficients  $\alpha$ ,  $\beta$ , and  $\gamma$  are used for a trade-off among terms on the evolution of the front. The algorithm requires two images as input: the initial shape which is corresponding to an initial zero-level set  $\varphi(\mathbf{p}, t = 0)$  and a feature image which is the image to be segmented. In this scheme, the initial zero-level set employs the surface which is represented by the isovalue of the initial shape. The propagation term for the evolution of the front is an edge potential image. With this image, the front moves rather fast in the low gradient regions and very slow in the high gradient regions. The evolution is terminated when the root-mean-square error change of the level set function is below a predefined threshold or the number of iterations reaches a predetermined number.

## Evaluation criteria

The performance evaluation process was performed by comparing the liver volumes computed by our proposed scheme

to the “gold standard” ones. We computed the true-positive rate (TP), true-negative rate (TN), false-positive error (FP), and false-negative error (FN). The accuracy and the Dice coefficient, which represents the fraction of volume overlapping between two volumetry approaches, were given by

$$\text{Accuracy} = (|TP| + |TN|) / (|TP| + |TN| + |FP| + |FN|), \tag{11}$$

$$\text{Dice} = \frac{2 |TP|}{|FP| + 2 |TP| + |FN|}, \tag{12}$$

The Dice coefficient is 100% for the perfect segmentation and 0% if the segmentation results by two approaches do not overlap at all. This is one of the most popular metrics for evaluating the accuracy of segmentation. In addition, the sensitivity, specificity, and the volume percentage error ( $E$ ) were also calculated as

$$\text{Sensitivity} = |TP| / (|TP| + |FN|), \tag{13}$$

$$\text{Specificity} = |TN| / (|TN| + |FP|), \tag{14}$$

$$E = |(V_c - V_g) / V_g|, \tag{15}$$

where  $V_c$  and  $V_g$  are the computerized volume and the gold standard volume, respectively.

The agreement between our measurement method and the gold standard reference method was expressed by the Pearson product-moment correlation coefficient ( $\rho$ ) which is widely used as a measurement of the degree of linear dependence between two variables. This coefficient is zero for no correlation, and one if two variables are total positive correlation. The statistical significance analysis of correlation was performed by using the Student’s  $t$ -test. The reliability analysis of measurements was performed by using the intraclass correlation coefficient (ICC) [15]. It was assumed that all  $n$  cases were chosen randomly, and all cases were rated by  $k$  raters (volume measurement methods). The models of two-way random single and average measures,  $ICC(2,1)$  and  $ICC(2,k)$ , were applied. They were calculated by:

$$ICC(2, 1) = \frac{MS_C - MS_{CR}}{MS_C + (k - 1)MS_{CR} + k(MS_R - MS_{CR})/n}, \tag{16}$$

$$ICC(2, k) = \frac{MS_C - MS_{CR}}{MS_C + (MS_R - MS_{CR})/n}, \tag{17}$$

where  $MS_C$ ,  $MS_R$ , and  $MS_{CR}$  are the mean square for between cases, between raters, and interaction, respectively. The statistically significant results were obtained by using the variance analysis.

## Results and discussion

The results of intermediate steps in our proposed scheme are illustrated in Fig. 2. The denoising technique, which uses the anisotropic diffusion, was applied to the original 3D MR image (Fig. 2a). It should not only smooth the image, but also preserve the major structures including the liver boundaries as depicted in Fig. 2b. The smoothed image was used to generate the gradient magnitude image by using a recursive Gaussian filter (Fig. 2c). The watershed, connected component, and relabeled filter were applied to produce the relabeled regions (Fig. 2d). Then, the liver candidate region and its features were determined. The thresholding method was performed to produce the thresholding image (Fig. 2e). The thresholding image was updated, and then, the boundaries of the liver were enhanced as depicted in Fig. 2f. The region with the largest volume was filtered out, and the morphological operations were applied to generate the rough shape of the liver (Fig. 2g). This rough shape was refined by using a geodesic active contour model to obtain the segmented liver as depicted in Fig. 2h. The liver segmentation obtained by our fully automatic scheme (white contour) was compared with the “gold standard” segmentation (black contour) as shown in Fig. 2i.

A comparison between the manual tracing method and the computerized method was performed. Table 1 represents the mean and deviation of the liver volumes obtained from two measurement methods. The average volume measured by the fully automated scheme was  $1456 \pm 392\text{cm}^3$ , and the average volume measured by the manual tracing method was  $1567 \pm 437\text{cm}^3$ . The mean volume percentage error was 8.3%. The overall means of accuracy and Dice coefficients were  $99.0 \pm 2.5$  and  $91.1 \pm 1.9\%$ , respectively. Those of sensitivity and specificity were  $88.10 \pm 3.3$  and  $99.70 \pm 0.2\%$ , respectively. The Pearson correlation coefficient on the measured volumes of two volumetry methods was 0.98 which was a positive correlation with not statistically significant ( $t$ -value = 24.98). Two volumetry methods obtained an agreement with high intraclass correlation coefficients. The intraclass correlation for mean rating,  $ICC(2,k)$ , was 0.97 with a 95% confidence interval of (0.94, 0.99). The intraclass correlation for a single rater,  $ICC(2,1)$ , was 0.94 with a 95% confidence interval of (0.88, 0.97). The results from the ICC analysis are shown in Table 2.

Figure 3 illustrates the liver segmentation results of our proposed scheme for a case which has the high Dice coefficient. Our computerized segmentation agreed excellently with the gold standard reference segmentation for slices which contain the liver portion as depicted in Fig. 3b, d. Another case with the Dice coefficient close to the average Dice value is shown in Fig. 4. Overall, our fully automated scheme for liver segmentation offered accurate results compared to those obtained from the gold standard method. How-



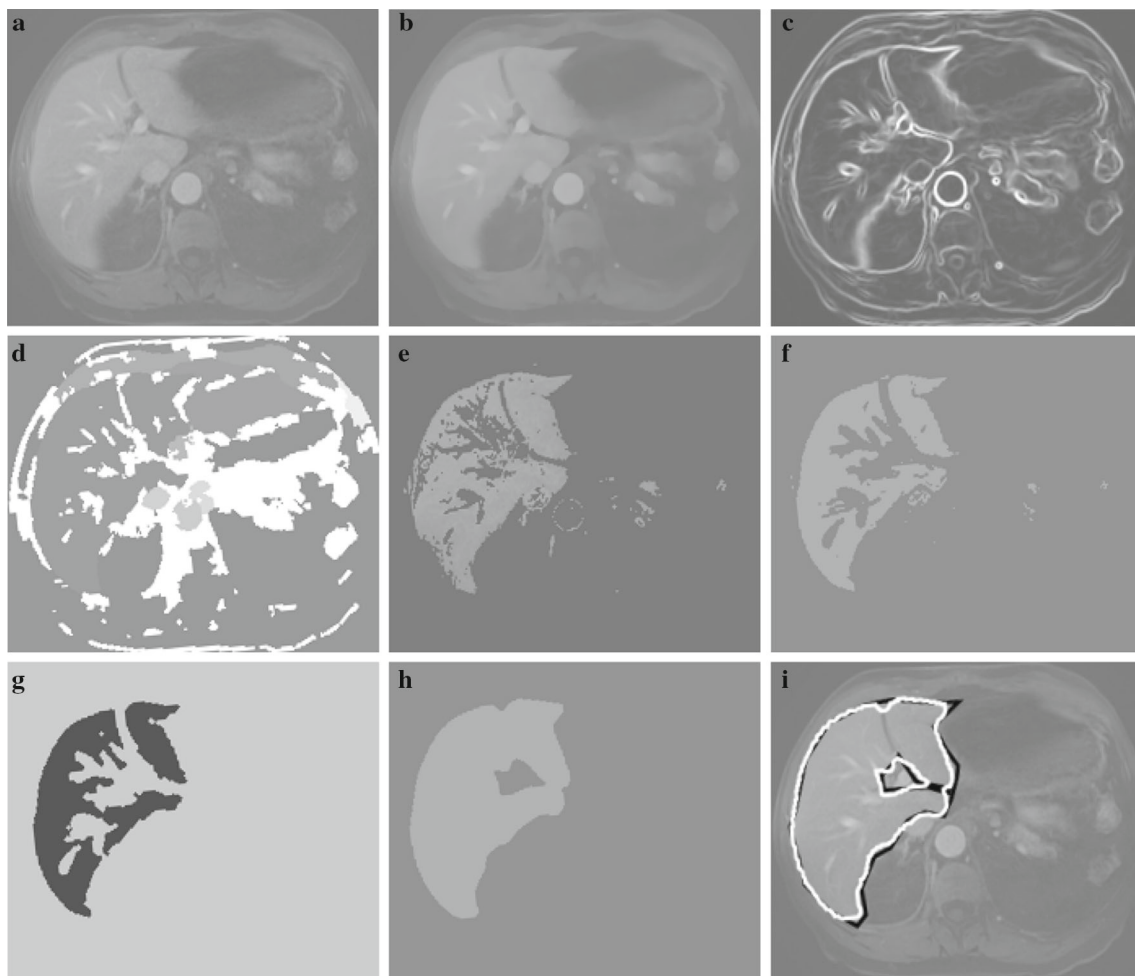


**Fig. 2** An illustration of the results of intermediate steps in our fully automated computerized scheme. **a** Original axial T1-weighted MR image of liver in portal venous phase. **b** Three-dimensional anisotropic diffusion reduction. Noise in image is reduced substantially, whereas major structures in liver, such as major vessels and liver boundaries, are maintained. **c** Three-dimensional recursive Gaussian filter.

**d** The relabeled regions after applying a watershed transform and connected-component filter. **e** The thresholding method. Two thresholds are automatically determined. **f** The boundaries of the liver were enhanced. **g** The initial shape of liver. **h** Three-dimensional active contour segmentation. **i** Computer-based segmentation (*white contour*) and reference-standard manual liver segmentation (*black contour*)

**Table 1** Comparison between our fully automated liver volumetry (computer volume) and gold standard volumetry (manual volume)

	Average	Standard deviation
Computer volume (cc)	1456	392
Manual volume (cc)	1567	437

ever, there exist over- and under- segmentations in the segmented liver occasionally. The major sources of FP and FN are shown in Fig. 5. The major FNs were caused by intensity variations or lesions on the surface of the liver. The major FPs were caused by the vena cava, heart, colon, stomach, or kidney, which adjoin to the liver. They were also from convex or concave parts of the boundaries which have high curvatures. In addition, the partial volume effects also caused some FPs.

**Table 2** Analysis of variance table from intraclass correlation coefficient analysis

	<i>df</i>	Sum of squares	Mean squares	F
Between raters	1	167,784	167,784	38.4
Between cases	26	8,878,568	341,483	78.2
Within cases	27	281,280	10,417	
Residual	26	113,496	4,365	
Total	53	9,159,848		

*df* degree of freedom, *F* *F* statistic value

The average time for a case was 8.4 min on PC (Intel, Xeon, 2.66GHz) by using the proposed liver segmentation scheme, while that was 24.7 min by using the manual tracing method. The difference was statistically significant ( $p < 0.001$ ).

**Fig. 3** Comparisons between our fully automated computerized liver volumetry (*white contours*) and the gold standard manual volumetry (*black contours*) for a case (68-year-old man) with a high Dice coefficient (94.7%). **a** An axial MRI slice. **b** A computer contour (*white*) and a manual contour (*black*). **c** A different axial slice of the same patient. **d** A computer contour (*white*) and a manual contour (*black*)

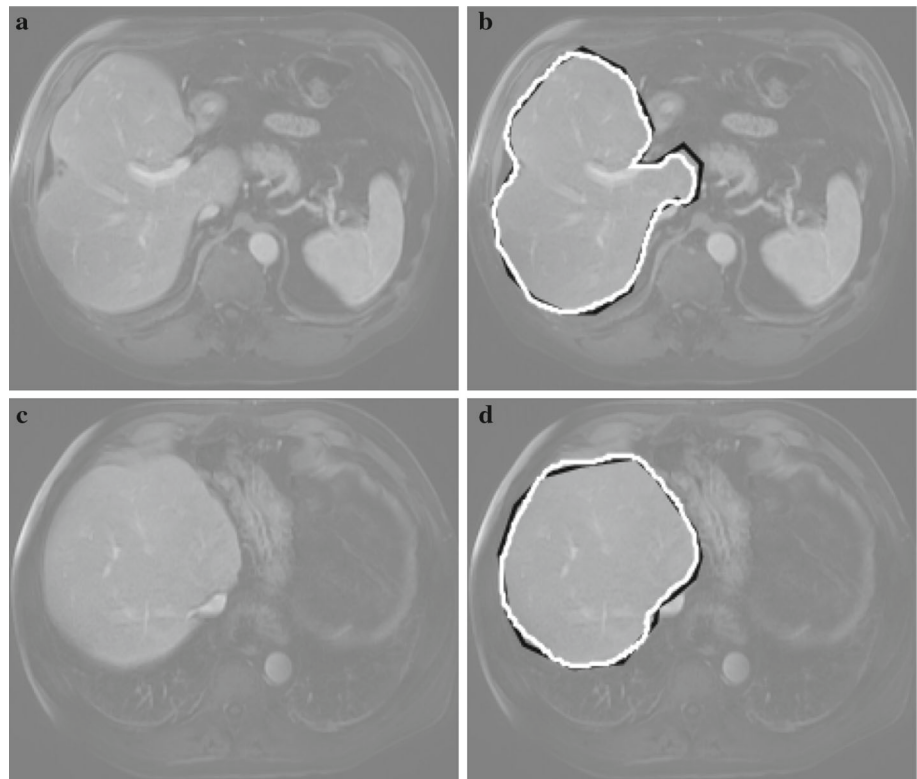


**Fig. 4** Comparisons between our fully automated computerized liver volumetry (*white contours*) and the gold standard manual volumetry (*black contours*) with a case (another 68-year-old man) with a Dice coefficient of 90.1% which is close to the average Dice coefficient (91.1%). **a** An axial MRI slice. **b** A computer contour (*white*) and a manual contour (*black*). **c** A different axial slice of the same patient. **d** A computer contour (*white*) and a manual contour (*black*)

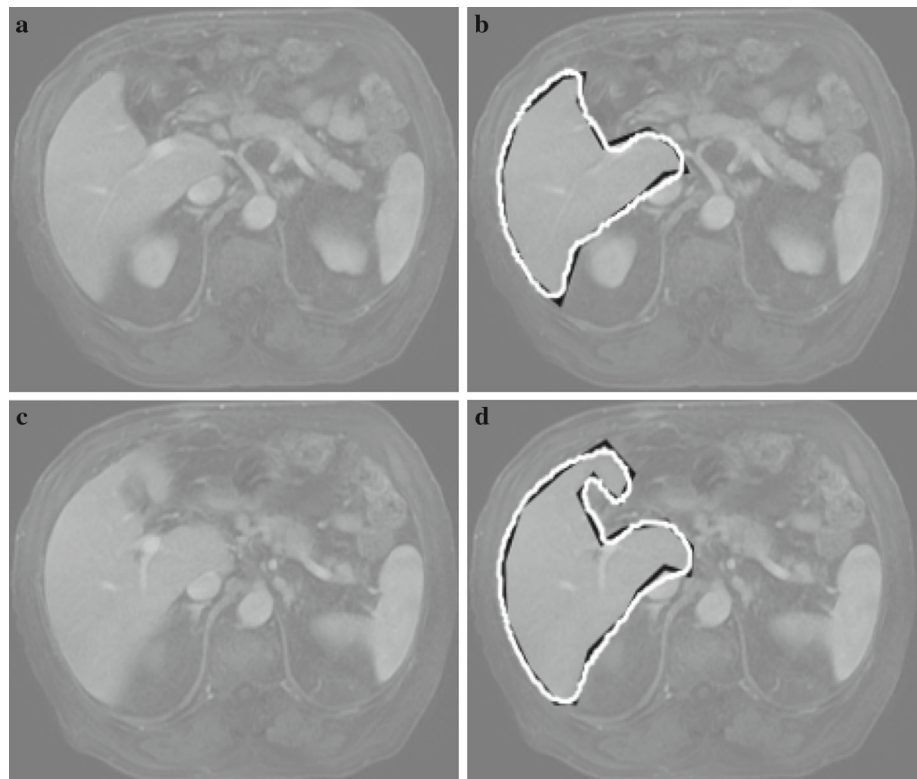
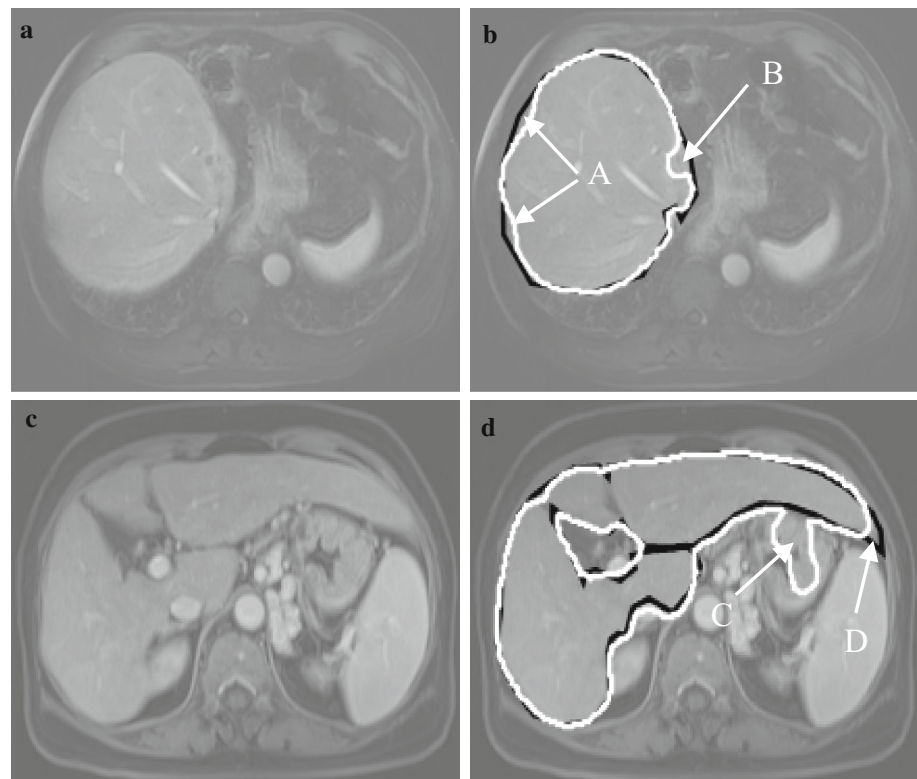


**Fig. 5** Illustrations of major false-positive (FP) and false-negative (FN) sources in two cases (**a, b** 68-year-old man with cancer; **c, d** 75-year-old woman with cancer). **a** An axial MRI slice of a patient (68-year-old man with cancer). **b** A computer contour (*white*) and a manual contour (*black*). In panel **b** there are FNs due to low-intensity (*A*) and lesion on liver boundary (*B*). **c** An axial MRI slice of another patient (75-year-old woman with cancer). **d** A computer contour (*white*) and a manual contour (*black*). In panel **d** there is an FP due to a part of the colon (*C*) and a FN (*D*) due to a high curvature region on the boundary



There are several user-defined parameters for the proposed scheme. These parameters were determined by empirical analysis on one case, and they were fixed for all remaining cases. Hence, our scheme is robust.

It is not easy to directly compare the proposed method with other existing methods in the literature due to differences in datasets and quality measurements. In CT volumetry, the approach proposed by Seghers et al. [2] obtained the overlap error of 10.7% for a publicly available database (SLIVER07). The approach represented by Florin et al. [16] yielded a 10.72% error in liver volume. The method developed by Freiman et al. [17] obtained the volume percentage error of 5.36% for their database, and the error for the SLIVER07 dataset was 2.36%. In MR images, the method proposed by Gloger et al. [7] for liver volumetry obtained volume percentage error of 11.8% for fatty livers and the error for normal livers was 8.3%. The processing time of this method for fatty and normal livers was 15.4 and 11.2 min, respectively.

As in previous studies, the limitation in this study is the number of expert radiologists who traced the manual contour. It will be ideal if the gold standard measurement were produced by multiple experienced radiologists. However, there were no many centers or institutions which can satisfy this requirement. Although several investigators have reported the performance evaluation based on the gold standard measurement, none of them employed the measurements from multiple-radiologist measurements. Even though there are multiple experienced radiologists, the inter-observation vari-

ability among them is small and the correlation coefficient between manual volumes was reported as 0.997 [18]. Given a small inter-observer variation, we believe that the liver volumes carefully obtained by a single expert radiologist should serve as the gold standard.

## Conclusions

The liver segmentation in MR abdominal images is one of challenging tasks. Only a few attempts have been made to address this issue, while MRI is increasingly used as an exam for liver resection and transplantation. This leads to imperative demands for developing computerized MRI liver volumetry. Existing schemes required interactions by users such as regions of interest or initial seed points, and a fully automated scheme has not been developed adequately due to its technical challenge. In this study, we rose to the challenge and developed a fully automated scheme for liver volumetry on 3D MR images. Our developed scheme employed the watershed transform, the statistical characteristics of liver, thresholding, and active contour algorithm. Our scheme does not require any interaction by or input from users. The volumes determined by our proposed scheme and the gold standard manual volumetry agreed excellently with an intra-class correlation coefficient of 0.94. Thus, the performance of our fully automated scheme was comparable to that of radiologists. The running time was 8.4 min per case on aver-



age. Our fully automated scheme saved radiologists' time for manual liver volumetry of 24.7 min per case.

**Acknowledgements** This research is funded by the Vietnam National Foundation for Science and Technology Development (NAFOSTED) under grant number 102.01-2013.47.

#### Compliance with ethical standards

**Conflict of interest** The authors declare that they have no conflict of interest.

**Research involving human participants** All procedures performed in studies involving human participants were in accordance with the ethical standards of the institutional and/or national research committee and with the 1964 Helsinki declaration and its later amendments or comparable ethical standards. This article does not contain any studies with animals performed by any of the authors.

**Informed consent** Informed consent was obtained from all individual participants included in the study.

## References

- Radtke A, Sotiropoulos GC, Nadalin S, Molmenti EP, Schroeder T, Lang H, Saner F, Valentin-Gamazo C, Frilling A, Schenk A, Broelsch CE, Malagó M (2007) Preoperative volume prediction in adult living donor liver transplantation: how much can we rely on it? *Am J Transpl* 7(3):672–9
- Seghers D, Slagmolen P, Lambelin Y, Hermans J, Loeckx D, Maes F, Suetens P (2007) Landmark based liver segmentation using local shape and local intensity models. In: *Proc MICCAI Workshop 3-D Segmentat. Clinic: a grand challenge*, pp 135–142
- Li G, Chen X, Shi F, Zhu W, Tian J, Xiang D (2015) Automatic liver segmentation based on shape constraints and deformable graph cut in CT images. *IEEE Trans Image Process* 24(12):5315–5329
- Suzuki K, Epstein ML, Kohlbrenner R, Garg S, Hori M, Oto A, Baron RL (2011) Quantitative radiology: automated CT liver volumetry compared with interactive volumetry and manual volumetry. *Med Phys Inform AJR* 197:W706–W712
- Göçeri E, Zübeyir M, Dicle O (2013) A comparative performance evaluation of various approaches for liver segmentation from SPIR images. *Turk J Electr Eng Comput Sci (TJEECS)* 23:741–768
- Göçeri E (2016) Fully automated liver segmentation using Sobolev gradient-based level set evolution. *Int J Numer Methods Biomed Eng*. doi:10.1002/cnm.2765
- Gloger O, Kühn J, Stanski A, Völzke H, Puls R (2010) A fully automatic three-step liver segmentation method on LDA-based probability maps for multiple contrast MR images. *Magn Reson Imaging* 28:882–897
- Rusko L, Bekes G (2011) Liver segmentation for contrast-enhanced MR images using partitioned probabilistic model. *Int J Comput Assist Radiol Surg* 6:13–20
- Masoumi H, Behradb A, Pourminaa MA, Roosta A (2012) Automatic liver segmentation in MRI images using an iterative watershed algorithm and artificial neural network. *Biomed Signal Process Control* 7:429–437
- Huynh HT, Karademir I, Oto A, Suzuki K (2014) Computerized liver volumetry on MRI by using 3D geodesic active contour segmentation. *Med Phys Inform AJR* 202:152–159
- Le TN, Bao PT, Huynh HT (2015) Fully automatic scheme for measuring liver volume in 3D MR images. In: *The 4th international conference on biomedical engineering and biotechnology (ICBE2015)*, pp S1361–S1369
- Suzuki K, Horiba I, Sugie N (2003) Linear-time connected-component labeling based on sequential local operations. *Computer Vis Image Underst* 89:1–23
- He L, Chao Y, Suzuki K, Wu K (2009) Fast connected-component labeling. *Pattern Recognit* 42:1977–1987
- Caselles V, Kimmel R, Sapiro G (1997) Geodesic active contours. *Int J Computer Vis* 22:61–79
- Portney LG, Watkins MP (1993) *Foundations of clinical research: applications to practice*, 2nd edn. Appleton and Lange, Norwalk
- Florin C, Paragios N, Funka-Lea G, Williams J (2007) Liver segmentation using sparse 3D prior models with optimal data support. *Inf Process Med Imaging* 20:38–49
- Freiman M, Eliassaf O, Taieb Y, Joskowicz L, Azraq Y, Sosna J (2008) An iterative Bayesian approach for nearly automatic liver segmentation: algorithm and validation. *Int J Comput Assist Radiol Surg* 3:439–446
- Sandrasegaran K, Kwo PW, DiGirolamo D, Stockberger SM Jr, Cummings OW, Kopecky KK (1999) Measurement of liver volume using spiral CT and the curved line and cubic spline algorithms: reproducibility and interobserver variation. *Abdom Imaging* 24:61–65